POLITECNICO DI TORINO
Repository ISTITUZIONALE

ELM divertor peak energy fluence scaling to ITER with data from JET, MAST and ASDEX upgrade

Original
ELM divertor peak energy fluence scaling to ITER with data from JET, MAST and ASDEX upgrade / Eich, T., Sieglin, B., Thornton, A.J., Faitsch, M., Kirk, A., Herrmann, A., Suttrop, W., Subba, F., Jet, C.. - In: NUCLEAR MATERIALS AND ENERGY. - ISSN 2352-1791. - 12:(2017), pp. 84-90. [10.1016/j.nme.2017.04.014]

Availability:
This version is available at: 11583/3017330 since: 2026-11-01T15:21:19Z

Publisher:
Elsevier Ltd

Published
DOI:10.1016/j.nme.2017.04.014

Terms of use:

This article is made available under terms and conditions as specified in the corresponding bibliographic description in the repository

Publisher copyright

(Article begins on next page)

25 November 2026

Nuclear Materials and Energy 12 (2017) 84–90

Contents lists available at ScienceDirect

Nuclear Materials and Energy

journal homepage: www.elsevier.com/locate/nme

ELM divertor peak energy fluence scaling to ITER with data from JET, MAST and ASDEX upgrade

T. Eich[a,*], B. Sieglin[a], A.J. Thornton[b], M. Faitsch[a], A. Kirk[b], A. Herrmann[a], W. Suttrop[a], JET contributors[c,1], MST contributors[c,2], ASDEX Upgrade and MAST teams[c]

[a] Max-Planck-Institut für Plasmaphysik, Garching, Germany
[b] CCFE, Culham Science Centre, Oxfordshire OX14 3DB, United Kingdom
[c] EUROfusion Consortium, JET, Culham Science Centre, Abingdon, OX14 3DB, UK

ARTICLE INFO

Article history:
Received 19 September 2016
Revised 21 March 2017
Accepted 22 April 2017
Available online 29 May 2017

ABSTRACT

A newly established scaling of the ELM energy fluence using dedicated data sets from JET operation with CFC & ILW plasma facing components (PFCs), ASDEX Upgrade (AUG) operation with both CFC and full-W PFCs and MAST with CFC walls has been generated. The scaling reveals an approximately linear dependence of the peak ELM energy with the pedestal top electron pressure and with the minor radius; a square root dependence is seen on the relative ELM loss energy. The result of this scaling gives a range in parallel peak ELM energy fluence of 10–30 MJm^{-2} for ITER Q= 10 operation and 2.5–7.5 MJm^{-2} for intermediate ITER operation at 7.5 MA and 2.65 T. These latter numbers are calculated using a numerical regression ($\varepsilon_{II} = 0.28 \frac{MJ}{m^2} n_e^{0.75}\ T_e^1\ \Delta E_{ELM}^{0.5}\ R_{geo}^1$). A simple model for ELM induced thermal load is introduced, resulting in an expression for the ELM energy fluence of $\varepsilon_{II} \cong 6\pi\ p_e\ R_{geo}\ q_{edge}$. The relative ELM loss energy in the data is between 2–10% and the ELM energy fluence varies within a range of $10^{0.5} \sim 3$ consistently for each individual device. The so far analysed power load database for ELM mitigation experiments from JET-EFCC and Kicks, MAST-RMP and AUG-RMP operation are found to be consistent with both the scaling and the introduced model, ie not showing a further reduction with respect to their pedestal pressure. The extrapolated ELM energy fluencies are compared to material limits in ITER and found to be of concern.

© 2017 The Authors. Published by Elsevier Ltd.
This is an open access article under the CC BY-NC-ND license.
(http://creativecommons.org/licenses/by-nc-nd/4.0/)

1. Introduction

The extrapolation of the ELM induced heat loads to larger devices such as ITER, which are foreseen to be operated in type-I ELMy H-Mode plasmas, is a crucial activity since it defines the operational range of future devices as well as the need for mitigation techniques [1,2]. The usually cited material limit for ELM peak divertor thermal impact is quoted to be 0.5 MJ/m^2 [3]. The latter value is an energy fluence and typically related to a nominally flat surface e.g. fully axisymmetric divertor target plates. Recent work by Gunn takes into account the castellation of the ITER divertor and finite ion orbit effects causing tungsten monoblock edge melting for the estimation of an acceptable ELM energy fluence in ITER [4].

In this work we take a pragmatic approach in assessing the heat load in future devices. We focus solely on the peak of the ELM energy fluence profile as this quantity will define the operational range and compares directly to the material limits. The ELM energy fluence profile is the temporal integration of the ELM heat flux profiles over the ELM duration (typically between 0.75 ms and 3 ms) [5].

The numbers for the peak ELM energy fluence have to be complemented by knowledge on the timescale of the ELM heat loads. Various works have investigated the ELM time scales for power loads in JET, ASDEX Upgrade (AUG) and MAST [6]. Here we will only summarize these findings as the database used for the new studies and presented in this paper are largely identical [7].

The analysis uses a new approach that directly compares the pedestal top plasma quantities, relative ELM losses and peak ELM energy fluence on the outer divertor target plates. A description of

* Corresponding author.
E-mail address: thomas.eich@ipp.mpg.de (T. Eich).

[1] See the Appendix of F Romanelli et al., Proceedings of the 25th IAEA Fusion Energy Conference 2014, Saint Petersburg, Russia.

[2] See the author list of "Overview of progress in European Medium Sized Tokamaks towards an integrated plasma-edge/wall solution" by H. Meyer et al., to be published in Nuclear Fusion Special issue: overview and summary reports from the 26th Fusion Energy Conference (Kyoto, Japan, 17–22 October 2016).

http://dx.doi.org/10.1016/j.nme.2017.04.014
2352-1791/© 2017 The Authors. Published by Elsevier Ltd. This is an open access article under the CC BY-NC-ND license. (http://creativecommons.org/licenses/by-nc-nd/4.0/)

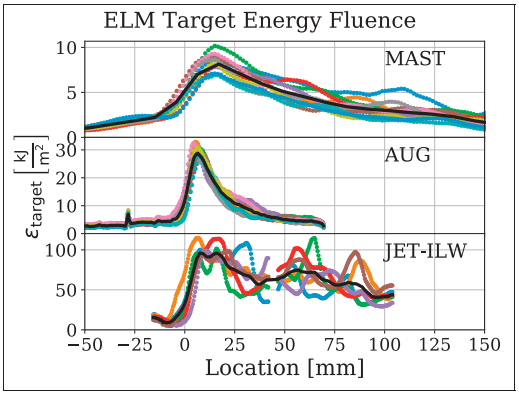

Fig. 1. Profiles of the ELM target energy fluence for 10 individual ELMs and an averaged profile (black line) for each device, which is MAST (#30,378), AUG(#32,338) and JET–ILW(#83,334) from top to bottom.

the experimental approach and the database is given in Section 2. In Section 3 the data will be used for regression studies. Equipped and motivated by the regression law for the ELM peak energy fluence, we introduce a simple model in Section 4 that explains the main characteristics of the newly found scaling, notably enabling not only the correct parametric dependence but also shows fair agreement with the absolute range of values. The major uncertainty of both the regression and the model is the variation of a factor ~3 due to the ELM loss size which will be discussed in Section 5. Section 6 will briefly apply the model prediction to a selected discharge with ELM mitigation. Section 7 will compare to the material limits in ITER and provide a more general discussion.

2. Measurements and data base for JET, MAST and ASDEX upgrade

The work presented here uses measurements of the pedestal top density and electron temperature taken from ECE and TS for JET and TS solely for AUG and MAST. These profiles are fitted using the standard fitting techniques for pedestal profiles, e.g. see [8–10]. All data are in Lower-Single-Null configurations with the ion BxGrad(B) drift direction downwards. Here we only use the pedestal top electron density and the pedestal top electron temperature in a time window just prior to the ELM. The relative ELM energy loss is calculated by using diamagnetic measurements for JET on the plasma stored energy at the beginning and the end of the ELM event. For AUG and MAST the W_{MHD} is used from equilibrium reconstruction. Additionally only global discharge parameters like the toroidal and poloidal magnetic field at the outer mid plane and plasma geometry enter our analysis.

Fig. 1 shows an example of the divertor ELM peak energy fluence profile for each device [5–7,11]. The ELM energy fluence, ϵ_{II}, is calculated by integrating the heat flux profile measured by infrared (IR) thermography for the duration of an ELM event (definition see [7]).

$$\varepsilon_{II}(s) = \int_{t_ELM} q_{II}(s,t)dt$$

$$q_{II} = \frac{q_{div} - q_0}{\sin(\alpha_{div})}$$

$$\varepsilon_{II}^{peak} = \max(\varepsilon_{II}(s))$$

The inclination angle of the field lines onto the divertor target is denoted as α_{div}. It should be noted that this procedure is performed for coherently averaged ELMs using the time of peak power as the common reference time and subtracting the inter-ELM heat flux profile q_0. We compare the divertor ELM peak energy fluence with pedestal measurements, which are recorded by Thomson-Scattering (TS) at a comparably low temporal resolution. All data points correspond to the period between 75 and 95% of the ELM cycle. An extension towards single ELM analysis is not envisaged here due to the low temporal TS resolution for all devices.

A survey of the discharge parameters and pedestal parameters is given in Table 1. We distinguish here between JET-C with carbon plasma facing components (PFCs), JET-ILW with ITER-like-wall (ILW) operation, AUG-C for ASDEX Upgrade operation with carbon wall (both divertor and first wall) and AUG-W for the operation with solely tungsten as PFCs. MAST operates only with carbon PFCs and provides a further benchmark to the model since it has (a) comparably low pedestal temperatures and (b) is a spherical tokamak.

The time scales of the ELM heat load in the divertor were intensively studied by using the presented database [5,7]. An earlier description is given by work from ASDEX Upgrade, MAST and JET by Herrmann [6]. Latter studies conclude that the rise time of the ELM heat pulse will be τ_{rise}=250 µs in ITER, given by the sound speed of 4700 eV pedestal ions and the connection length from the outboard mid plane to the divertor in the burning plasma scenario. The heat pulse is described in fair approximation by a triangular waveform with a decay time $\tau_{decay} = 2 \times \tau_{rise}$ in line with the free-streaming-particle approach [12,13]. We briefly note that the work providing the material limits [3,4] also used the power load temporal shape defined by τ_{rise}=250 µs and τ_{decay}=500 µs.

For lower values of the pedestal temperature at half field/half current, the rise time is increased by the factor $\sqrt{4700eV/2350eV}=\sqrt{2}$ as it refers to the ion sound speed ($c_s \sim \sqrt{T_i+T_e}$) to reflect the smaller ion thermal speed resulting in 350µs. As this number enters only with a square root dependence for the material limit due to the underlying thermal expansion (e.g. causing cracking) the overall relief is only about $\sqrt[4]{2}\approx 1.2$ and, as a result, is ignored for further discussion.

3. Empirical scaling of the ELM energy fluence

We apply standard least square fitting techniques to derive a regression law for the parallel ELM energy fluence. Uncertainties of the heat flux measurements do not enter the statistical analysis. As regression parameters, we chose the pedestal top electron density $n_{e,ped}$, the pedestal top electron temperature $T_{e,ped}$, the relative ELM size ($\Delta E_{ELM}=E_{ELM}/W_{Plasma}$) and for the linear machine dimension both the geometrical major radius R_{geo} and a_{geo}. Using the ansatz for best fitting

$$\varepsilon_{II} = C_\varepsilon * n_{e,ped}^{\alpha} T_{e,ped}^{\beta} \ \Delta E_{ELM}^{\gamma} R_{geo}^{\delta} \quad (1)$$

Table 1
Survey on discharge parameters for the five data sets used in this work.

	B_{tor}	I_p	q_{95}	R	A	$n_{e,ped}$	$T_{e,ped}$	ΔE	#
Unit	T	MA	–	m	M	$10^{19}m^{-3}$	keV	%	–
JET-C	1.5–3.2	1.5–3.5	2.7–5.3	2.9	0.94	2.7–7.4	0.5–2.3	2.7–9.5	40
JET-ILW	1.0–3.1	1.0–3.5	2.6–6.1	2.9	0.93	1.9–8.8	0.3–1.3	3.0–9.4	96
AUG-C	2.0–2.5	0.8–1.2	3.8–4.8	1.62	0.5	3.6–4.2	1.2–1.7	3.3–7.2	3
AUG-W	2.5–2.6	0.8–1.1	3.6–4.9	1.62	0.5	3.6–6.0	0.6–0.9	4.0–6.6	11
MAST	0.4–0.55	0.39–0.44	3.0–5.1	1.02	0.53	2.3–3.9	0.1–0.2	1.8–6.6	24

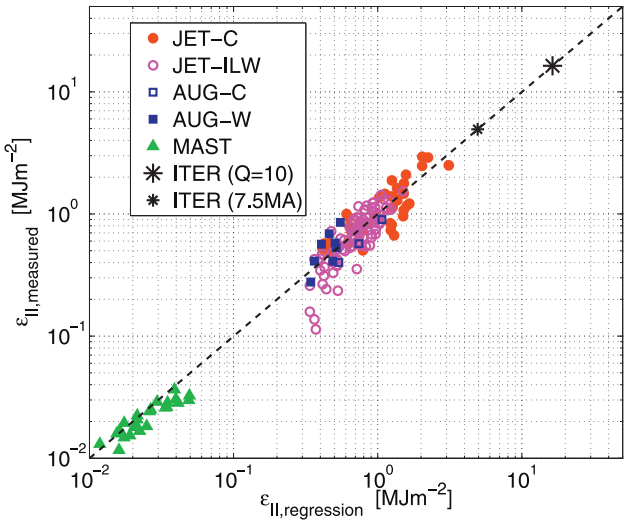

Fig. 2. Regression of the outer divertor parallel ELM energy fluence for JET, MAST and AUG as parameterized in Eq. (2). A good description of the data is achieved with a systematic span of about a factor of ~3. Both ITER operational points are shown and result in 16.3 MJ/m^2 for Q= 10 (15 MA/5.3 T) and 4.9 MJ/m^2 for half field/half current (7.5 MA/2.65 T) with ELM sizes of 5.4% for both cases.

results in the following empirical scaling ($R^2 = 0.82$) for the parallel ELM energy fluence with the density $n_{e,ped}$ expressed in units of [10^{20} m^{-3}], $T_{e,ped}$ in [keV], ΔE_{ELM} in [%] and R_{geo} in [m].

$$\varepsilon_{II} = 0.28 \pm 0.14 \frac{MJ}{m^2} \times n_{e,ped}^{0.75\pm0.15} \times T_{e,ped}^{0.98\pm0.1} \times \Delta E_{ELM}^{0.52\pm0.16} \times R_{geo}^{1\pm0.4} \quad (2)$$

Fig. 2 shows a comparison of the measured data and the data calculated using Eq. (2). Repeating the exercise with the minor machine radius, a_{geo}, results in practically the same powers in the scaling ($R^2 = 0.83$) except for the constant that is about a factor R_{geo}/a_{geo} larger:

$$\varepsilon_{II} = 0.90 \pm 0.29 \frac{MJ}{m^2} \times n_{e,ped}^{0.74\pm0.15} \times T_{e,ped}^{0.96\pm0.1} \times \Delta E_{ELM}^{0.5\pm0.15} \times a_{geo}^{1.05\pm0.38} \quad (3)$$

From Eqs. (2) and (3) we see that the ELM energy fluence is about proportional to pedestal top pressure as well as to the linear machine size and dependent on the square root of the relative ELM size. As an explanation for this we assume that the divertor heat load is dominated by parallel transport of reconnected or edge ergodized flux tubes. This is in line with JOREK simulation [14,15] as well as earlier experimental work on the ELM heat load deposition pattern [16]. Once a flux tube connects the pedestal top region with the divertor plate through ergodized field lines, the pedestal volume drains towards the divertor target plates depositing there the major fraction of the ELM loss energy that is given by the pedestal pressure (which can be written in units of [Jm^{-3}]) and the length of the flux tube in the pedestal region (which is in the unit of [m]). Since we compare the peak energy fluence to the top (*peak*) pedestal values for n_e and T_e, we reveal a clear correlation. Finally we note that using the pedestal top electron pressure, relative ELM size and minor radius we get a scaling $\varepsilon \sim p^{0.9}\Delta E^{0.5}a^1$. The remaining scatter of the data is in the range of ~3. We will come back to this remaining uncertainty in Section 5.

The product of the machine size, e.g. the minor radius, and the pedestal pressure will give a quantity with the dimensions $p_e \times a_{geo} = [Jm^{-3}] \times [m] = [Jm^{-2}]$. As a result of the regression analysis, we construct a model for the absolute peak ELM energy fluence on the basis that it is described by the product $p_e \times a_{geo}$. This leaves us with the square root dependence to be discussed in Section 5 in conjunction with the remaining scatter of the data of about a factor of 3 which is notably small compared to the achieved range of about 100 for the quantity of interest.

The extrapolation to ITER conditions is summarized in Table 2 both for Q= 10 (15 MA/5.3 T) and half field/half current (7.5 MA/2.65 T) parameters. As the pedestal values for ITER are discussed in this contribution, we only vary the relative ELM size, with the results summarized in Table 2. The relative ELM sizes chosen are the lowest, the mean and the highest values in the observed data set. We note that the squre-root dependence should be handled with care as outlined in more detail in Section 5.

The ELM peak energy fluence values, when extrapolated to ITER, range from about 10 MJm^{-2} to 30 MJm^{-2} as estimated by both the regression studies as well as the model prediction. A typical conversion factor due to the inclination angle of the castellated JET-ILW divertor between parallel and target heat fluxes is 10–12. Even under optimistic considerations using a conversion factor of 10 (as in JET-ILW) and small natural ELMs of 2%, a resulting 1 MJm^{-2} ELM peak energy fluence is found which is about twice the reported material limit of 0.5 MJm^{-2}. We further discuss the implications in Section 7.

MAST has a significantly different aspect ratio than JET or AUG. This is in general a good way to get information on the dependence on R/a. Given this, it is striking that scaling with R_{geo} (Eq. (2)) and a_{geo} (Eq. (3)) are nearly identical in all parameters. It would be worthwhile to explore further which is the more relevant variable. When we exclude the MAST data from the regression we find no significant change of the presented scaling nor for the projected values in ITER. Surely a more sophisticated regression analysis is necessary including an adequate treatment of the number of available data and their uncertainties is required. The comparison of the ELM energy fluence versus the ELM loss energy in Section 5 shows a restricted coverage of the operational range

Table 2
Survey on extrapolations to ITER for the ELM parallel peak energy fluence for the lowest, mean and highest observed relative ELM loss energies. Also included are the values for the lower, mean and upper boundary following the model predictions.

ITER, B_{tor}= 5.3T, I_p=15 MA (Q= 10)		ITER, B_{tor}= 2.65T, I_p= 7.5 MA	
$n_{e,ped} = 8 \times 10^{19}$ m^{-3}	$T_{e,ped}$ = 4700 eV	$n_{e,ped} = 4 \times 10^{19}$ m^{-3}	$T_{e,ped}$ = 2350 eV
Regression studies (Section 3)			
ΔE= 10%	22.53 MJm^{-2}	ΔE= 10%	6.7 MJm^{-2}
ΔE= 5.4%	16.3 MJm^{-2}	ΔE= 5.4%	4.9 MJm^{-2}
ΔE= 2%	9.7 MJm^{-2}	ΔE= 2%	2.9 MJm^{-2}
Model prediction (Section 4)			
3:1	28.1 MJm^{-2}	3:1	7.0 MJm^{-2}
2:1	18.8 MJm^{-2}	2:1	4.6 MJm^{-2}
1:1	9.4 MJm^{-2}	1:1	2.3 MJm^{-2}

when compared to JET. Without identifying the reason or hidden parameter for the remaining factor ~3, here and in the next section, we assume not be able to resolve if R_{geo} or a_{geo} is the more appropriate quantity.

4. Model for the ELM peak energy fluence

In the following section we construct a simple model for the peak ELM energy fluence. To be applicable to the presented database showing estimates from three different machines and 5 different divertor geometries, we choose a model for the energy fluence parallel to field lines. Basically all we are doing is a power balance for a toroidally uniform volume that spans a radial region of a small width d around the pedestal top position. We assume this volume to be connected along field lines due to ergodization to the divertor target plates. In such a situation, similar to the idea of the plug-in model by Janeschitz [17], the energy in the affected volume will be emptied by parallel transport. The time scale of the energy arriving at the target plate will be given by the free-streaming-particle approach [12,13] already mentioned in Section 2.

The ELM peak energy fluence on the divertor target is given by the energy, $E_{ped,top}$, in a toroidally uniform volume defined by two flux surfaces at a distance $\pm d/2$ around the pedestal top position, $V_{ped,top}$, which is divided by the corresponding area, A_{target}:

$$\varepsilon_{target} = \frac{E_{ped,top}}{A_{target}} = \frac{V_{ped,top}\ 3\ n_{e,ped,top}\ \ T_{e,ped,top}}{2\pi R_{target}\ d\ f_x\ 2} \tag{5}$$

with f_x being the flux expansion. An additional factor of two is found in the denominator to account for the existence of two divertor targets (outer/inner). Additionally some simplifications are introduced which could easily be replaced. However, to underline the heuristic nature of our attempt we use $T_e=T_i$, $Z_{eff}=1$, $R_{target}=R_{inner}=R_{outer}=R_{geo}$.

The volume is defined as

$$V_{ped,top} = 2\pi R_{geo}\ \times\ 2\pi a_{geo} \times \sqrt{\frac{1+\kappa^2}{2}} \times\ d\ \times\ \Delta_{equi} \tag{6}$$

The quantity Δ_{equi} is a geometrical factor calculated from magnetic equilibrium reconstruction, which is about 1.9 for both ASDEX Upgrade and JET and about 2.3 for MAST. The plasma elongation is denoted as κ. We use B_{tor} and B_{pol} for the toroidal and poloidal magnetic field at the outer mid plane and express the parallel energy fluence as

$$\varepsilon_{II} = \varepsilon_{target} \cdot \sin^{-1}(\alpha_{div}) = \varepsilon_{target} \cdot \frac{B_{tor}}{B_{pol}} \cdot f_x \tag{7}$$

We now combine Eqs (5+6+7) to arrive at:

$$\varepsilon_{II} = \Delta_{equi}\ \cdot 2\pi a_{geo}\sqrt{\frac{1+\kappa^2}{2}} \times \frac{3}{2} \cdot n_{e,ped,top} \cdot k_B \cdot T_{e,ped,top} \times \frac{B_{tor}}{B_{pol}} \tag{8}$$

Eq. (8) resembles both the linear dependence on the pedestal pressure as well as the linear dependence on the machine dimension. Noting that for our three devices Δ_{equi} is about ~2 and that an edge cylindrical safety factor is given by $q_{edge}=\sqrt{\frac{1+\kappa^2}{2}} \cdot \frac{a_{geo}}{R_{geo}} \cdot \frac{B_{tor}}{B_{pol}}$ we rewrite Eq. (8) in a compact form as

$$\boldsymbol{\varepsilon_{II}} \cong 6\pi\ \boldsymbol{p_e\ R_{geo}\ q_{edge}} \tag{9}$$

When defining a representative connection length for the edge region as $L_c=2\pi\ R_{geo}\ q_{edge}$ we can express Eq. (9) alternatively as

$$\boldsymbol{\varepsilon_{II}} = \boldsymbol{L_c}\ 3\boldsymbol{p_e}\frac{\Delta_{equi}}{2} \cong \boldsymbol{L_c}\ 3\boldsymbol{p_e} \tag{10}$$

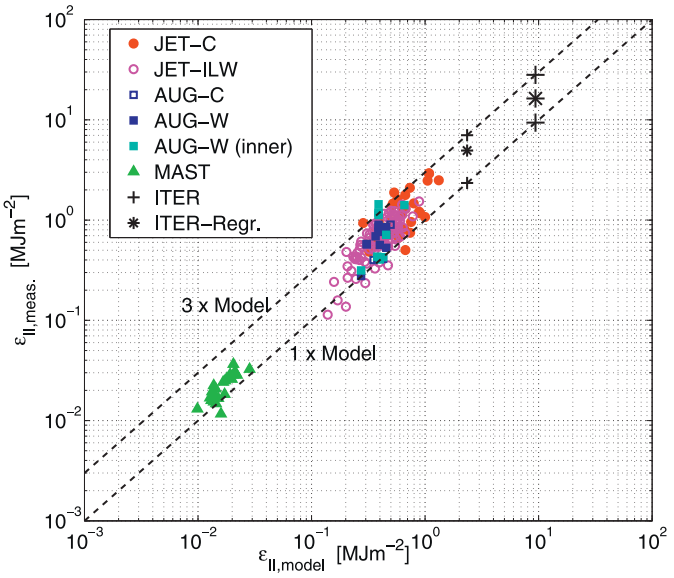

Fig. 3. Model prediction versus the database. The bottom numbers gives typical pedestal parameters. Some of the few available data points from the inner divertor in AUG are added.

The latter expression resembles the simple picture from which we have started, though now highlighting the form of a single flux tube reconnected to the target plates and snaking around the pedestal region. However, it should be noted that we do not describe a length in nature but still the volume of a flux tube projected on an area in the divertor and that the factor Δ_{equi} ~2 is cancelled out by the presence of the two divertor target plates.

In other words we fill a flux tube of the above defined connection length with plasma and which drains to both targets equally. Hence the model is only dependent on the magnetic flux surface geometry given by the correction factor Δ_{equi}, describing the widening between flux surfaces at the active x-point, but otherwise only depends on the parallel connection length. Arriving here, we note that the extra factor of 3 seen in the data possibly arises for large ELMs because then the reconnected flux tube snakes for up to three turns poloidally. This naive reasoning needs to be checked, of course, with sophisticated modelling attempts such as using the JOREK code. Fig. 3 shows a comparison of the database with the model prediction using Eq. (8). In the figure we draw an additional line showing a 3 times larger estimate (3:1) than the model predicts (1:1) and find that all data falls within these 1:1 and 3:1 lines. Thus we identify also a factor of three as found in the empirical scaling law. Note that the model is an absolute prediction. It gives a good description of the lower boundary of the data range for all three devices ranging more than a factor of 100 in ε_{II}. Finally we clarify that the width d of the flux tube is not believed to be significantly changed at the outer mid plane region due to an ergodic process, as such a process is the result of very small changes in the radial magnetic field of the order $B_{radial}/B_{tor} \sim 10^{-3}$.

Table 1 shows the results of the model applied for the two ITER cases. Comparing to the regression value we see that the lower (1:1) and upper model boundaries (3:1) are similar to the regression values for the largest and smallest ELMs in the database.

5. Remaining uncertainty due to the relative ELM size

Here we present some more details on the remaining factor of three and its correlation to the relative ELM size. The relative ELM size is defined as the ELM loss energy normalized to the plasma stored energy $\Delta E=E_{loss}/W_{plasma}$. The regression studies

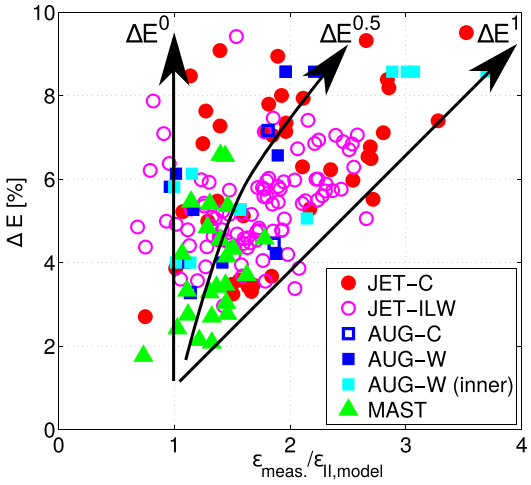

Fig. 4. The distribution of the relative ELM size versus the proximity to the model. The data are unequally distributed spanning a triangle. As a consequence the regression results in a square-root dependence on the relative ELM size.

give a square root dependence on ΔE. The remaining uncertainty of the regression values when applied to the database is slightly less than a factor of 3. The model prediction does not account for the actual ELM loss energy but gives a lower value for all observed data, notably also leaving an uncertainty of a factor of about 3. Fig. 4 shows the measured ε_{II} normalized to the model prediction $\varepsilon_{II,model}$ versus the relative ELM size. It can be seen that the distribution of the ELM sizes versus the normalized parallel ELM energy densities is unequally filled. Data close to the 3:1 line are rare and only existent for large ELMs, with relative ELM losses at about 7–9%. Interestingly data at the 1:1 ratio of measured versus model data, the points fill out the entire range of ELM size from 1.7% towards the highest number at about 10%. This triangle-like distribution is of importance to understand the regression results. The regression studies report $\varepsilon_{II} \sim \sqrt{\Delta E}$ which is possibly a statistical effect due data coverage. Dedicated scans of ELM sizes are desirable while maintaining constant pedestal pressures as best as possible, e.g. by moderate gas puffing. A further obvious candidate is to check the conductive/convective fractions of the ELM losses and of course the mode numbers of the ELM instabilities manifesting themselves as striations. These mode numbers are experimentally accessible by the so-called Quasi-Mode-Number from IR data [18,19]. First attempts to order the data by conductive and convective loss fractions at various neoclassical electron pedestal collisionalities did not reveal a clear picture, possibly due the simultaneous change of the ELM instability at low collisionalities [20].

6. Application to ELM mitigated plasmas

Fig. 5(a) shows the time trace of the stored energy, W_{MHD}, pedestal electron pressure $p_{e,ped}$ and the ELM induced parallel energy fluence $\varepsilon_{||}$ of an ELM mitigated discharge with Resonant Magnetic Perturbation (RMP) [22,23] in ASDEX Upgrade (#32080, $B_{tor} = -2.5$T, $I_p = 0.8$ MA, $P_{aux} \approx 7.5$ MW). The yellow shaded areas indicate the periods in the discharge with active external magnetic perturbation., light blue is the reference period before RMP is switched on. It is seen that all three quantities are reduced during phases with external magnetic perturbation compared to the unperturbed phases. The reduction of ELM induced energy fluence $\varepsilon_{||}$ is correlated to a reduction of the pedestal pressure. Fig. 5(b)+ 5(c) shows the measured relative ELM loss energy parallel ELM energy fluence in comparison to the model prediction. The database from the unmitigated discharges in ASDEX Upgrade, MAST and JET are shown for comparison. It is seen that both cases with and without external magnetic perturbation are captured within the prediction of the model. The observed reduction of the ELM energy fluence in the presence of external magnetic perturbations is explained largely by a reduction in pedestal pressure. Therefore, studies for ELM mitigation should report on any reduction of the pedestal pressure and assess the extent to which the ELM peak energy fluence is reduced in comparison to the reduction of the pedestal top pressure. An important result when assessing ELM mitigation (an increase of the ELM frequency and a reduction of the ELM loss size) by our novel method is that the observed correlation of the ELM energy fluence to the pedestal pressure holds for all analysed mitigated discharges that were investigated so far including data with RMP in AUG and JET-EFCC. A limited number of MAST-RMP ELMs are also included and support the scaling, however, a larger, more extensive survey of RMP data should be made to validate the result further across the full range of RMP applied data. Hence we do not attempt to give a conclusion for ELM mitigation experiments in general. For many more ELM mitigation experiments target heat load data are either not available or not published. This is a research field that needs stronger support in the near future. However, we clearly state for all data analysed also in ELM mitigation experiments no exception was found outside the 1:1 – 3:1 when applying our model. However, this is possibly due to the limited range ELM sizes (2–10%) achieved in the analysed experiments including the mitigation experiments. Data from JET with EFCC for which a reduction of the pedestal pressure is not observed also do not show a reduction of the divertor ELM energy fluence. Work from JET using pellet injection also report that the peak heat flux is unchanged for constant pedestal pressure [21].

7. Discussion (implications for ITER) and conclusions

We report here on two basic achievements when trying to extrapolate the ELM heat load to future machines. The ELM parallel peak energy fluence is well described by the pedestal top pressure, the machine linear dimension and some proportionality to the relative ELM size with a remaining uncertainty of about ~3. Additionally to this empirical result we constructed a model based on an energy balance of a toroidally symmetric shell volume around the pedestal top position that gives the lower boundary of the observed data in absolute terms and resembles the empirical parametric dependencies closely. This lower limit is given in a very compact form as $\boldsymbol{\varepsilon_{II} \cong 6\pi\ p_e\ R_{geo}\ q_{edge}}$.

The predicted numbers from the scaling presented here for ITER in the Q= 10 scenario for the smallest uncontrolled ELMs observed in the data base (~2%) are around 10 MJm^{-2} for both the regression and the 1:1 model prediction, as shown in Table 2. To relate this to a surface heat load density on the ITER divertor targets requires that the real geometry of the target be properly accounted for. The original specification of a maximum $\Delta E_{ELM} = 0.6$ MJ for ITER [2], was based on the avoidance of full surface melting on perfectly aligned, unshaped, castellated tungsten divertor targets. It assumed, conservatively, that there would be no broadening of the ELM wetted area compared with the inter-ELM width and that there could be a maximum in-out asymmetry of a factor 2 between the peak ELM energy fluence arriving at the target strike points (based on sparsely available measurements).

This limit must now be re-examined both in the light of the new scaling proposed here (for the outer divertor) and of progress in the ITER tungsten divertor design, in which global target tilting and W monoblock front surface shaping is incorporated to protect misaligned edges arising from engineering tolerances. The current shaping baseline includes a 0.5° global target tilt angle and a nominal 1° bevel on the monoblock surface [24], giving a worst case total angle of incidence of $\alpha_{out} = 4.2°$ at the outer divertor strike point for the baseline Q = 10 burning plasma equilibrium at

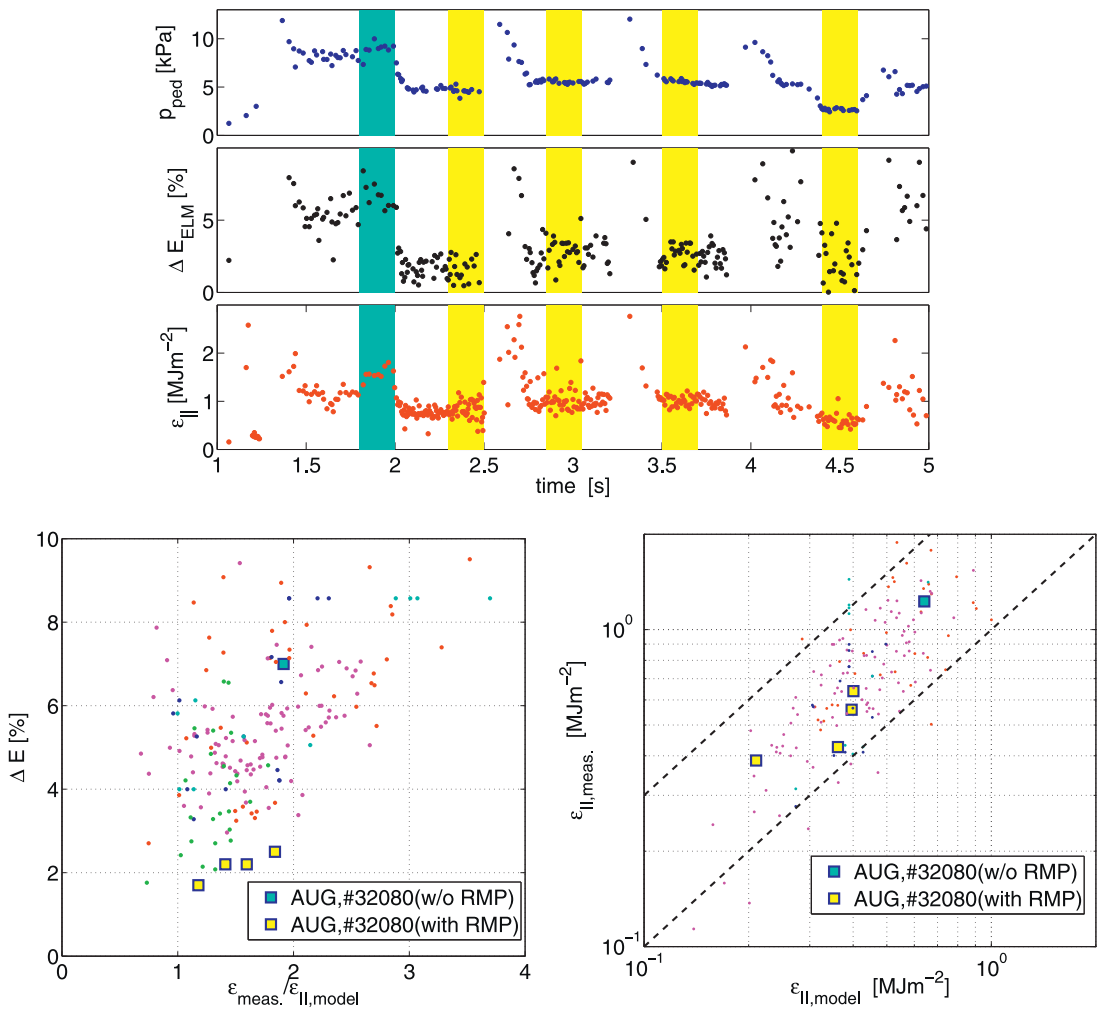

Fig. 5. (a) Influence of external magnetic perturbation on the pedestal pressure and ELM energy fluence in ASDEX Upgrade discharges. Light blue denotes the reference time before RMPs are applied, yellow denotes the intervals used for analysis and with RMPs switched on. (b) Reduction of ELM loss size and (c) reduction of the divertor ELM peak energy fluence.

$q_{95} = 3$ (the angle is slightly steeper $\alpha_{out} = 4.7$ at the inner target because of the higher target inclination). This gives a $\sin(\alpha_{out}) = 0.07$ factor transforming parallel heat flux density to a projected value perpendicular to the outer target surface ($\sin(\alpha_{in}) = 0.08$ at the inner strike point). Thus the $\varepsilon_{||} = 9.7\,\mathrm{MJm^{-2}}$ obtained from the regression for $\Delta E = 0.02$ in Table 2 would correspond to a peak perpendicular load of $\varepsilon_{\perp} \sim 0.7\,\mathrm{MJm^{-2}}$ which is marginally close to full surface melting for the expected burning plasma ELM temporal waveform, taking into account that the steady state tungsten surface temperature in the strike point region is expected to be of order 1000 °C. For $\Delta E = 0.1$, $\varepsilon_{||} = 22.5\,\mathrm{MJm^{-2}}$ from the regression (Table 2), and $\varepsilon_{\perp} \sim 1.6\,\mathrm{MJm^{-2}}$, yielding full surface flash melting at every ELM, leading to severe and unacceptable damage of the top surface after only a few plasma discharges [25].

At $I_p = 7.5$ MA, the scaling predicts $\varepsilon_{||} = 6.7\,\mathrm{MJm^{-2}}$ for $\Delta E = 10\%$, giving $\varepsilon_{\perp} < 0.5\,\mathrm{MJm^{-2}}$ (assuming the same q_{95}), opening up the possibility that even the largest uncontrolled ELMs may be marginally tolerable with regard to surface melting during the non-active phase or early D or DT phase operation at half current. It should be noted, however, that full surface melting may not ultimately set the final limit on tolerable ELM sizes in ITER. Although individual divertor monoblock shaping protects leading edges between toroidally adjacent units, new 3D ion orbit calculations in support of the ITER shaping design find that the toroidal gap edges between poloidally adjacent monoblocks can locally melt during ELMs, even if the top surface does not [4]. In addition, any asymmetries between the inner and outer divertor ELM loading would also lower the allowed ELM energy drop. In fact, the database presented here is currently being extended to include data from the inner divertor region for all three devices currently contributing to the scaling. Very first results from AUG using some newer, dedicated IR systems were already included in Fig. 4 and are in line with the prediction of the parallel ELM parallel peak energy fluence onto the outer divertor. It is finally important to note that material studies in which ITER-grade tungsten is subjected in electron beam facilities to large numbers of fast, low amplitude transients indicate that fatigue generated surface cracking can occur far below any melting threshold [26]. Ultimately, it is such mechanical limits, which may set the allowable ΔW_{ELM}.

In relation to the need reduce ELM target energy densities, new measurements we have performed so far during ELM mitigation experiments are also found to follow the same scaling as for the uncontrolled ELMs. The observed reduction of the ELM energy fluence in the presence of external magnetic perturbation compared to the situation without the perturbation is explained mostly by a reduction in pedestal pressure due to the application of the fields.

To refine the scaling and better understand the controlling physics beyond the first result presented here, a better understanding of $\varepsilon \sim \Delta E^{\alpha}$ (with α being between 0 and 1) is mandatory. This

is particularly important in the sense that the new scaling predicts peak energy densities for high performance burning plasmas which, for the smallest ELMs in the database, are not too far above the limits dictated by surface melting. To reduce the energy fluence to acceptable levels would, according to the scaling, require Type I ELMs at the level of $\Delta E = 0.1–0.5\%$, which are not naturally observed. It may, however, be possible, to further reduce the target energy fluence by buffering in a highly radiative divertor plasma (which ITER must anyway achieve at $Q = 10$ if steady state power flux densities are to be manageable), provided the initial ELM amplitude is sufficiently small.

One of the highest priorities for further research in this area in the near future is to examine Type-I ELM scenarios on current devices (with confinement sufficient for $Q = 10$ operation on ITER) and study whether conditions can be found with smaller ELMs ($\Delta E < 0.5\%$) or in the presence of detachment and/or high SOL radiation fractions to allow reduction of the ELM energy fluence. It is also important that other devices add measurements to the database, including if possible points for both inner and outer divertor.

Acknowledgement

This work has been part funded by the RCUK Energy Programme [grant number EP/P012450/1]. This work has been carried out within the framework of the EUROfusion Consortium and has received funding from the Euratom research and training programme 2014–2018 under grant agreement No 633053. The views and opinions expressed herein do not necessarily reflect those of the European Commission.

The authors thank R.A.Pitts from IO for fruitful discussions.

References

[1] A.W. Leonard, et al., Phys. Plasmas 21 (2014) 090501.
[2] A. Loarte, et al., Nucl. Fus. 54 (2014) 033007.
[3] J. Linke, et al., Nucl. Fus. 51 (2011) 073017.
[4] J. Gunn, these proceedings.
[5] B. Sieglin, et al., Plasma Phys. Control. Fus. 55 (2013) 124039.
[6] A. Herrmann, et al., J. Nucl. Mater. 313-316 (2003) 759.
[7] T. Eich, et al., J. Nucl. Mater. 415 (2011) S856–S859.
[8] M.N.A. Beurskens, et al., Nucl. Fus. 49 (2009) 125006.
[9] R.J. Groebner, et al., Nucl. Fus. 41 (2001) 17892001.
[10] R. Scannell, et al., Rev. Sci. Instrum. 82 (2011) 053501.
[11] A.J. Thornton, et al., Nucl. Fus. 54 (2014) 064011.
[12] T. Eich, et al., J. Nucl. Mater. 390-391 (2009) 760–763.
[13] W. Fundamenski, et al., Plasma Phys. Control. Fusion 48 (2006) 109–156.
[14] G.T.A. Huysmans, et al., Plasma Phys. Control. Fusion 51 (2009) 124012.
[15] S. Pamela, et al., Plasma Phys. Control. Fus. 58 (2015) 014026.
[16] T. Eich, et al., Phys. Rev. Lett. 91 (2003) 195003.
[17] G. Janeschitz, et al., J.Nucl.Mater. 290–293 (2001) 1.
[18] T. Eich, et al., Plasma Phys. Control. Fus. 47 (2005) 815–842.
[19] A.J. Thornton, et al., Plasma Phys. Contr. Fus. 59 (2017) 014047.
[20] P.B. Snyder, Nucl. Fus. 44 (2004) 320–328.
[21] R. Wenninger, et al., Plasma Phys. Control. Fus. 53 (2011) 105002.
[22] W. Suttrop, et al., Phys. Rev. Lett. 106 (2011) 225004.
[23] A. Kirk, et al., Nucl. Fus. 55 (2015) 043011.
[24] S. Carpentier, et al., Phys. Scr. T159 (2014) 014002.
[25] R.A. Pitts, et al., these proceedings.
[26] M. Wirtz, et al., these proceedings.